LHCb-PUB-2024-009
May 5, 2025

Track momentum resolution measurement for Run 3 at LHCb

The LHCb collaboration[†]

Abstract

The long track momentum resolution is a key metric for evaluating the performance of the tracking system at LHCb. This document presents the methodology to measure the long track momentum resolution. The preliminary result using a subsample of the 2024 dataset is presented.

LHCb-PUB-2024-009
05/05/2025

© 2025 CERN for the benefit of the LHCb collaboration. CC BY 4.0 licence.

[†]Contact authors: zehua.xu@cern.ch, ya.zhao@cern.ch

Contents

1 Introduction

The LHCb detector [1–3] is a single-arm forward spectrometer covering the pseudorapidity range $2 < \eta < 5$, designed for the study of particles containing b or c quarks. The detector has been substantially upgraded prior to the Run 3 data-taking period, which started in 2022. The upgraded detector was designed to match the performance of the Run 1-2 detector, while allowing it to operate at approximately five times the instantaneous luminosity. The high-precision tracking system has been fully replaced and consists of a silicon-pixel vertex detector surrounding the pp interaction region (VELO) [4], a large-area silicon-strip detector (UT) [5] located upstream of a dipole magnet with a bending power of about 4 T m, and three stations of scintillating fibre detectors (SciFi) [5]. Different types of charged hadrons are distinguished using information from two ring-imaging Cherenkov (RICH) detectors [6, 7]. The entire photon detection system of the Cherenkov detectors has been renewed for the upgraded detector. Photons, electrons and hadrons are identified by a calorimeter system consisting of electromagnetic (ECAL) and hadronic (HCAL) calorimeters. Muons are identified by a system composed of alternating layers of iron and multiwire proportional chambers [8]. Readout of all detectors into an all-software trigger [9] is a central feature of the upgraded detector, allowing the reconstruction of events at the full LHC interaction rate, and their selection in real time. The trigger system is implemented in two stages: a first inclusive stage, based primarily on charged particle reconstruction, which reduces the data volume by roughly a factor of 20, and a second stage, which performs the full offline-quality reconstruction and selection of physics signatures. A large disk buffer is placed between the two stages to hold the data while the real-time alignment and calibration is being performed.

The track model in LHCb classifies the reconstructed tracks into five types according to which sub-detectors recorded charged clusters from the track: VELO track, T track, Long track, Upstream track and Downstream track [10]. Long tracks are the most critical set of tracks for physics analyses, as hadrons which contain beauty or charm quarks usually decay in the VELO volume and the resulting charged final states will form long tracks. These tracks traverse the entire tracking system, leaving clusters in both the VELO and the SciFi detectors, and optionally hits in the UT station. The reconstruction of long tracks starts from searching for VELO tracks which basically form straight lines since the VELO is sufficiently displaced from the magnetic field. Two algorithms, *forward tracking* and *track matching*, are used to join VELO tracks with SciFi hits and form long tracks [11]. The forward tracking starts with VELO tracks and extends them with SciFi clusters to form long tracks. The track matching algorithm uses a standalone track reconstruction algorithm to match and combine VELO tracks with T tracks to make long tracks [12, 13]. A track fit which is based on Kalman Filter technique is performed to obtain the best estimates of the momentum, positions and directions of tracks in the vertex region [14].

The track momentum resolution directly impacts the reconstruction of physics decay channels, and serves as a key metric for evaluating the performance of the tracking system at LHCb. In this note, only long tracks are used to study the track momentum resolution, as they pass through the full magnetic field and provide the most precise momentum estimates.

The momentum resolution for long tracks is determined using $J/\psi \to \mu^+\mu^-$ decays by measuring the dimuon mass resolution, which is primarily dictated by the momentum resolution of the two muons. Neglecting the muon masses and considering decays where

the two muons have similar momenta, the relative momentum resolution, σ_p/p, can be approximated as:

$$\frac{\sigma_p^2}{p^2} = 2\left(\frac{\sigma_m}{m}\right)^2 - 2\left(\frac{\sin\theta\sigma_\theta}{2-2\cos\theta}\right)^2$$

where m is the invariant mass of the J/ψ candidate and σ_m is the signal width obtained from a fit to the mass distribution. The second term is a correction for the opening angle, θ, between the two muons, where σ_θ is the per-event error on θ which is obtained from the track fits of the two muon tracks. The derivation of this equation is detailed in Section 2.1.

2 Formulas derivation and validation

The formula for calculating the track momentum resolution using a data-driven approach can be found in a previous LHCb paper [3]. However, this formula is not entirely accurate and not validated. In this chapter, we present a more precise formula for calculating the track momentum resolution, specifically using the dimuon mass resolution obtained from the $J/\psi \to \mu^+\mu^-$ decay. The validation of the formula using simulated samples is discussed in Section 2.2.

2.1 Formulas derivation

From the $J/\psi \to \mu^+\mu^-$ energy conservation we know:

$$E_{J/\psi} = E_{\mu^+} + E_{\mu^-} = \sqrt{p_+^2c^2 + m_\mu^2c^4} + \sqrt{p_-^2c^2 + m_\mu^2c^4} \tag{1}$$

Neglecting the μ mass:

$$E_{J/\psi} = p_+c + p_-c \tag{2}$$

Momentum conservation yields:

$$\vec{p}_{J/\psi} = \vec{p}_+ + \vec{p}_- \tag{3}$$

$$p_{J/\psi}^2 = p_+^2 + p_-^2 + 2p_+p_-\cos\theta \tag{4}$$

$$E_{J/\psi}^2 = m^2c^4 + p_{J/\psi}^2c^2 \tag{5}$$

Using Eq. (2), Eq. (4) and Eq. (5) $\Rightarrow$

$$m = \frac{\sqrt{p_+p_-}}{c}\sqrt{2-2\cos\theta} \tag{6}$$

$$\sigma_m^2 = \left(\frac{\partial m}{\partial p_+}\right)^2\sigma_{p_+}^2 + \left(\frac{\partial m}{\partial p_-}\right)^2\sigma_{p_-}^2 + \left(\frac{\partial m}{\partial \theta}\right)^2\sigma_\theta^2 \tag{7}$$

$$= m^2\frac{\sigma_{p_+}^2}{4p_+^2} + m^2\frac{\sigma_{p_-}^2}{4p_-^2} + m^2\frac{\sin^2\theta\sigma_\theta^2}{(2-2\cos\theta)^2} \tag{8}$$

Let $\sigma_{p_+}/p_+ = \sigma_{p_-}/p_-$

$$\frac{\sigma_p^2}{p^2} = 2\left(\frac{\sigma_m}{m}\right)^2 - 2\left(\frac{\sin\theta\sigma_\theta}{2-2\cos\theta}\right)^2 \tag{9}$$

The θ can be calculated using formulas below:

$$\theta = \arccos\left[\frac{t_{x_1}\cdot t_{x_2} + t_{y_1}\cdot t_{y_2} + 1}{\sqrt{t_{x_1}^2 + t_{y_1}^2 + 1}\cdot\sqrt{t_{x_2}^2 + t_{y_2}^2 + 1}}\right] \tag{10}$$

where t_x and t_y refer to the x component and y component of the track slope. Then σ_θ can be calculated through the partial derivatives with respect to t_x and t_y and the error propagation law:

$$\begin{aligned}
\sigma_\theta^2 &= \begin{pmatrix} \frac{\partial\theta}{\partial t_{x_1}} \\ \frac{\partial\theta}{\partial t_{y_1}} \\ \frac{\partial\theta}{\partial t_{x_2}} \\ \frac{\partial\theta}{\partial t_{y_2}} \end{pmatrix}^{\mathrm{T}} \cdot \begin{pmatrix} \sigma_{t_{x_1}}^2 & \mathrm{cov}(t_{x_1}, t_{y_1}) & 0 & 0 \\ \mathrm{cov}(t_{x_1}, t_{y_1}) & \sigma_{t_{y_1}}^2 & 0 & 0 \\ 0 & 0 & \sigma_{t_{x_2}}^2 & \mathrm{cov}(t_{x_2}, t_{y_2}) \\ 0 & 0 & \mathrm{cov}(t_{x_2}, t_{y_2}) & \sigma_{t_{y_2}}^2 \end{pmatrix} \cdot \begin{pmatrix} \frac{\partial\theta}{\partial t_{x_1}} \\ \frac{\partial\theta}{\partial t_{y_1}} \\ \frac{\partial\theta}{\partial t_{x_2}} \\ \frac{\partial\theta}{\partial t_{y_2}} \end{pmatrix} \\
&= \left(\frac{\partial\theta}{\partial t_{x_1}}\right)^2 \sigma_{t_{x_1}}^2 + 2\left(\frac{\partial\theta}{\partial t_{x_1}}\right)\left(\frac{\partial\theta}{\partial t_{y_1}}\right)\mathrm{cov}(t_{x_1}, t_{y_1}) + \left(\frac{\partial\theta}{\partial t_{y_1}}\right)^2 \sigma_{t_{y_1}}^2 \\
&\quad + \left(\frac{\partial\theta}{\partial t_{x_2}}\right)^2 \sigma_{t_{x_2}}^2 + 2\left(\frac{\partial\theta}{\partial t_{x_2}}\right)\left(\frac{\partial\theta}{\partial t_{y_2}}\right)\mathrm{cov}(t_{x_2}, t_{y_2}) + \left(\frac{\partial\theta}{\partial t_{y_2}}\right)^2 \sigma_{t_{y_2}}^2
\end{aligned} \tag{11}$$

The expression θ can also be calculated using the momentum direction:

$$\theta = \arccos\left[\frac{\frac{p_{x_1}}{p_{z_1}}\cdot\frac{p_{x_2}}{p_{z_2}} + \frac{p_{y_1}}{p_{z_1}}\cdot\frac{p_{y_2}}{p_{z_2}} + 1}{\sqrt{\left(\frac{p_{x_1}}{p_{z_1}}\right)^2 + \left(\frac{p_{y_1}}{p_{z_1}}\right)^2 + 1}\cdot\sqrt{\left(\frac{p_{x_2}}{p_{z_2}}\right)^2 + \left(\frac{p_{y_2}}{p_{z_2}}\right)^2 + 1}}\right] \tag{12}$$

However, θ should not directly depend on the momentum, thus this formula is not used to calculate the momentum resolution. It is still useful to validate the formula.

2.2 Validation of the formulas using MC samples

A large $J/\psi \to \mu^+\mu^-$ MC sample was generated using RapidSim [15] to validate Eq. (9). In the MC sample the true momentum is known, thus the momentum resolution can be obtained directly. Figure 1 shows that the results using two different methods are consistent, thus Eq. (9) is proved to be correct.

The calculation of θ and σ_θ should also be validated. Another $J/\psi \to \mu^+\mu^-$ MC sample using full LHCb detector simulation is used, which contains the information of the track state covariance matrix. Figure 2 shows that the formulas are correct.

In conclusion, the data-driven method to calculate the momentum resolution has been fully validated.

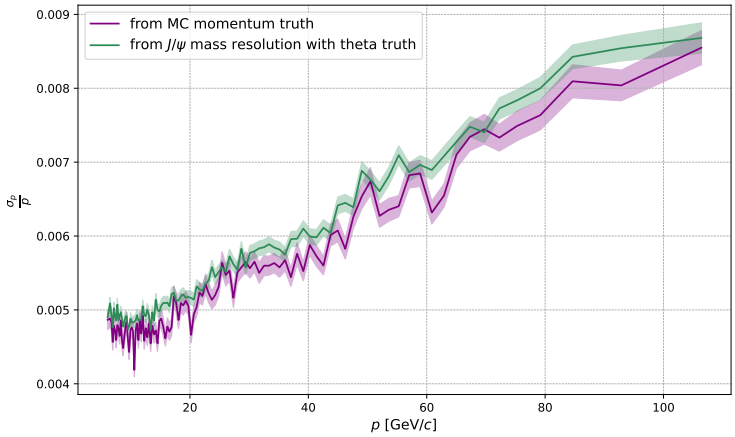

Figure 1: Purple line: momentum resolution using true momentum information, i.e. performing a Gaussian fit on the difference between the reconstructed momentum and the true momentum, and extracting the width as the momentum resolution. Green line: momentum resolution using Eq. (9), and Eq. (12) is used for the calculation of angle term, i.e. using the reconstructed momentum and the true momentum to calculate the reconstructed θ and true θ, then performing a Gaussian fit on the difference between the two and extract the width as the value of σ_θ.

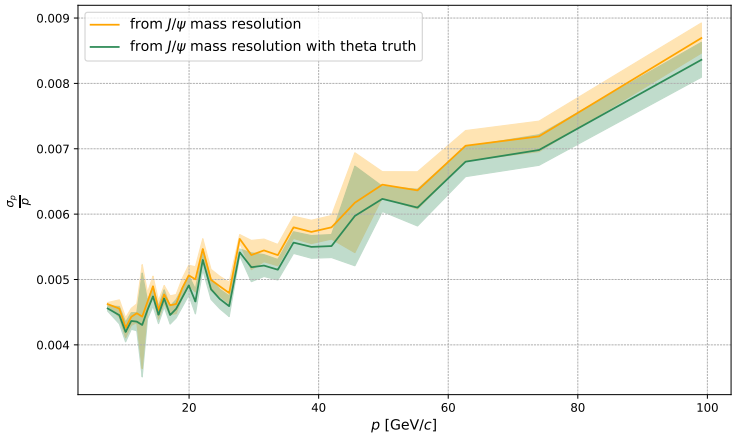

Figure 2: Green line: momentum resolution using Eq. (9), and Eq. (12) is used for the calculation of angle term, i.e. using the reconstructed momentum and the true momentum to calculate reconstructed θ and true θ, then performing a Gaussian fit on the difference between the two and extract the width as the σ_θ. Orange line: momentum resolution using Eq. (9), and Eq. (10) is used for the calculation of angle term, i.e. calculating θ using t_x and t_y, and applying the error propagation formula incorporating t_x error, t_y error, and their covariance to compute the value of σ_θ.

2.3 Track parameter errors correction

The calculation of σ_θ uses track parameter errors, so we need to check whether the track parameter errors are correctly assigned.

The distance of closest approach between two muon tracks, doca, which only depends on track parameters, can be used to check the correctness of the track parameter errors. If the track parameter errors are correct, then the distribution of the doca pull, $\frac{doca}{\sigma_{doca}}$, should be a standard normal distribution. However, Figure 3 shows that the width is larger than 1, thus the track parameter errors are underestimated and need to be corrected. Since σ_{doca} and σ_θ have the same origin, i.e. the VELO track parameter errors, and the vertex fitting procedure doesn't introduce additional errors, the scale factor measured from $\frac{doca}{\sigma_{doca}}$ can be used to correct σ_θ. Figure 4 shows the measured scale factors in each momentum bin.

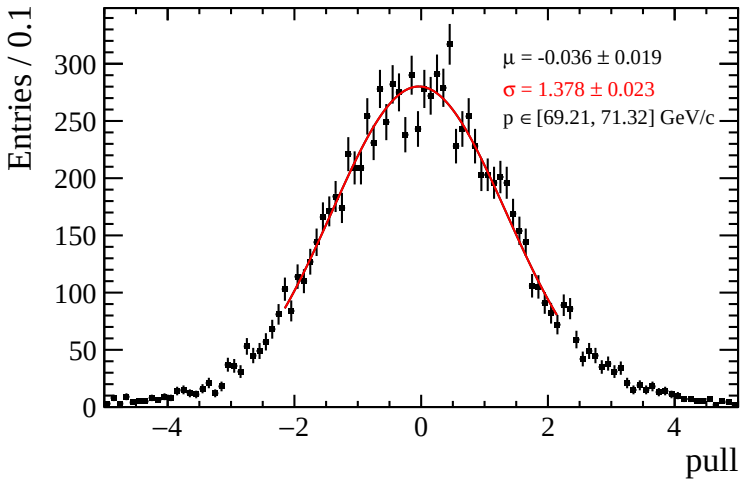

Figure 3: The distribution of $\frac{doca}{\sigma_{doca}}$ in one momentum bin. The width is larger than 1, thus σ_{doca} is underestimated.

3 Track momentum resolution using Run3 data

3.1 Triggers and selections

LHCb Run3 data collected in 2024 are used to study the track momentum resolution. A large amount of $J/\psi \to \mu^+\mu^-$ decays were collected from the data of fill number 9982-10056 (Run number 303094-304604).

A standard online and offline di-muon selection is applied to filter signal candidates. For the online selection, events are required to pass through the `Hlt1DiMuonHighMass` line at the HLT1 stage [9]. The `Hlt1DiMuonHighMass` line is triggered by a pair of high-momentum tracks identified as muons [16], which form a good-quality vertex and has a combined invariant mass larger than 2.7 GeV. The HLT2 trigger line `Hlt2JpsiToMuMu` is used to filter $J/\psi \to \mu^+\mu^-$ signals, the detailed selections are listed in Table. 1 and the definition of the variables used can be found in Appendix B.

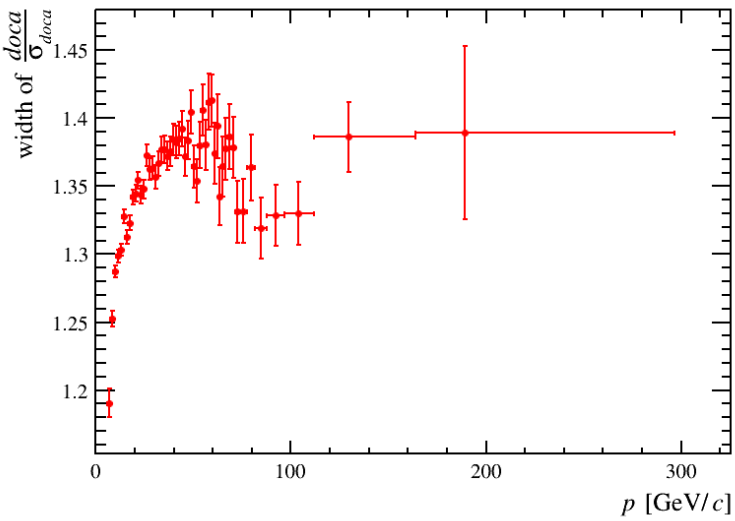

Figure 4: The scale factors in each momentum bin.

Table 1: Summary of HLT2 selection.

Event selection of `Hlt2_JpsiToMuMu` trigger line	
Requirement	Applied to
$p_{\mathrm{T}} > 0.3$ GeV	$\mu^{\pm}$ candidate
PID_MU > -5	$\mu^{\pm}$ candidate
$\lvert \mathrm{MASS} - 3096.9 \rvert < 150$ MeV	J/ψ candidate
CHI2DOF < 25	$\mu^{\pm}$ candidate
MINIPCHI2 > 0	$\mu^{\pm}$ candidate
MINIP > 0	$\mu^{\pm}$ candidate
ISMUON = 1	$\mu^{\pm}$ candidate
BPVDLS > 0	J/ψ candidate
DOCACHI2 < 10000	J/ψ candidate

Further cut-based selections are applied to improve the signal purity, with details documented in Table. 2.

An additional cut that the relative difference of the momentum of two muons is smaller than 1% is applied to fulfill the approximation condition. Finally there are about 2.74 million entries left after all cuts.

3.2 Momentum resolution calculation

The dataset is divided into 51 momentum regions. In each region, the distribution of $\frac{\sigma_p}{p}$ in a momentum region can be obtained using Eq. (9). The value of σ_m is extracted from the fit of the dimuon invariant mass, where the sum of a Crystal Ball function and an exponential function is used as the fit function. Figure 5 shows examples of the fit. The value of θ is calculated using Eq. (10), and σ_θ is calculated using Eq. (11), then corrected by a factor, as discussed in Section 2.3. The mean of $\frac{\sigma_p}{p}$ is taken as the momentum

Table 2: Summary of further offline selection.

Variable	Value
Vertex fit probability P(χ^2/ndf)	< 3
Ghost Probability of Muon	< 0.3
Muon p_{T}	$> 700\,\mathrm{MeV}/c$
Muon p	3 GeV/c $<$ p $<$ 500 GeV/c
Muon Identification	isMuon, $\mathrm{DLL}_{\mu\pi} > 0$
Mass cut	$\lvert m(\mu^+\mu^-) - M(J/\psi)\rvert < 150\,\mathrm{MeV}/c^2$
Pseudo proper time	$\lvert t_z\rvert < 10\,\mathrm{ps}$
Uncertainty of t_z	$< 0.3\,\mathrm{ps}$
J/ψ p_{T}	< 14 GeV/c
rapidity	$2 < y < 4.5$
number of PV	> 0
number of UTHits	> 0

resolution of this region, and the uncertainty of the mean is taken as the uncertainty of the momentum resolution.

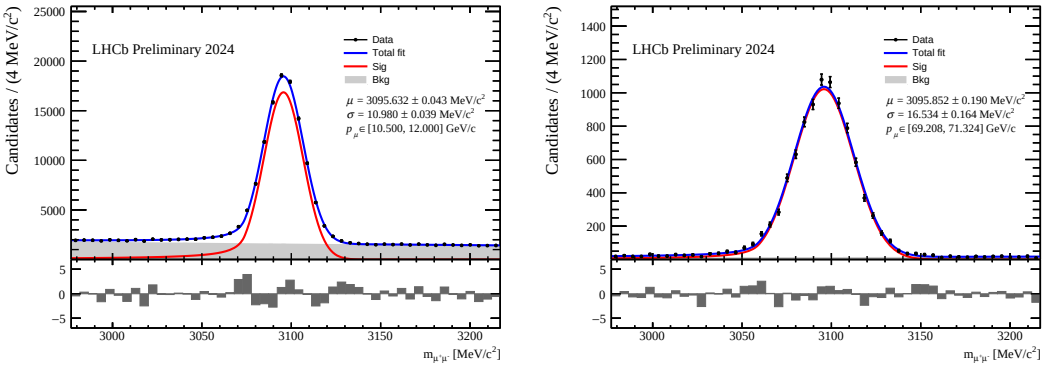

Figure 5: Fit of the invariant mass of $\mu^+\mu^-$ in a low momentum region (left) and a high momentum region (right). The fit function is composed of a Crystal Ball function (red curve) and an exponential function (gray shadow).

Finally we get the plot of the track momentum resolution with respect to the momentum, as shown in Figure 6, where the result from the simulation sample is also shown.

It can be seen that the resolution obtained from the simulation sample does not match very well with the one from data. In physics analyses, correcting the differences between data and simulation is important for obtaining more accurate results. Therefore, it is essential to smear the values in the simulation sample with the measured momentum resolution from data.

4 Summary and outlook

The methodology to measure the long track momentum was presented and the formulas were validated. To calculate the momentum resolution, the mass resolution from the fit of

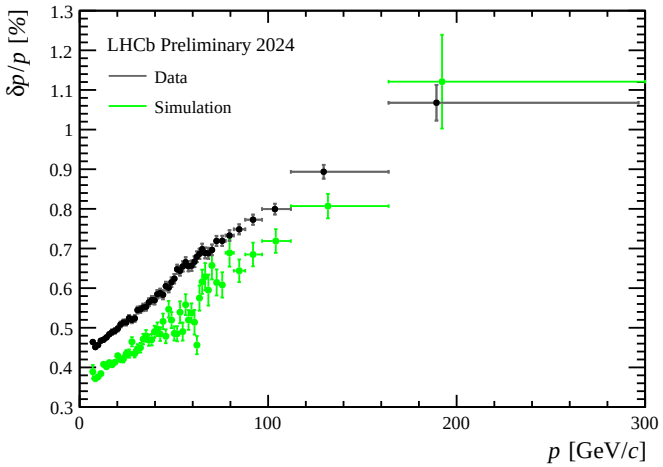

Figure 6: Gray: relative momentum resolution of long tracks as a function of momentum using $J/\psi \to \mu^+\mu^-$ data sample. Green: relative momentum resolution calculated using simulation sample.

the $\mu^+\mu^-$ invariant mass and the angle between the two muon tracks in the VELO and the angular resolution are needed. The track parameter errors used in the calculation of the angular resolution are underestimated and need to be corrected by a factor, which is just the width of the distribution of the doca pull. The preliminary result of the long track momentum resolution was presented, using a subsample of the 2024 dataset filtered by a two-stage trigger and cut-based selection. The result shows an improvement compared with the result of Run 1 [3].

We also expect that the momentum resolution could be further improved with a better magnet field description and finer track alignment. A final optimization could be achieved by performing a momentum scale calibration [17].

Acknowledgements

We express our gratitude to our colleagues in the CERN accelerator departments for the excellent performance of the LHC. We thank the technical and administrative staff at the LHCb institutes. We acknowledge support from CERN and from the national agencies: CAPES, CNPq, FAPERJ and FINEP (Brazil); MOST and NSFC (China); CNRS/IN2P3 (France); BMBF, DFG and MPG (Germany); INFN (Italy); NWO (Netherlands); MNiSW and NCN (Poland); MCID/IFA (Romania); MICIU and AEI (Spain); SNSF and SER (Switzerland); NASU (Ukraine); STFC (United Kingdom); DOE NP and NSF (USA). We acknowledge the computing resources that are provided by CERN, IN2P3 (France), KIT and DESY (Germany), INFN (Italy), SURF (Netherlands), PIC (Spain), GridPP (United Kingdom), CSCS (Switzerland), IFIN-HH (Romania), CBPF (Brazil), and Polish WLCG (Poland). We are indebted to the communities behind the multiple open-source software packages on which we depend. Individual groups or members have received support from ARC and ARDC (Australia); Key Research Program of Frontier Sciences of CAS, CAS PIFI, CAS CCEPP, Fundamental Research Funds for the Central Universities, and Sci. & Tech. Program of Guangzhou (China); Minciencias (Colombia); EPLANET, Marie Skłodowska-Curie Actions, ERC and NextGenerationEU (European Union); A*MIDEX, ANR, IPhU and Labex P2IO, and Région Auvergne-Rhône-Alpes (France); AvH Foundation (Germany); ICSC (Italy); Severo Ochoa and María de Maeztu Units of Excellence, GVA, XuntaGal, GENCAT, InTalent-Inditex and Prog. Atracción Talento CM (Spain); SRC (Sweden); the Leverhulme Trust, the Royal Society and UKRI (United Kingdom).

Appendices

A Changes after the track parameter errors correction

Figure 7 shows the change of the ratio between the θ term and the mass term in Eq. (9) and the change of momentum resolution after the correction was applied.

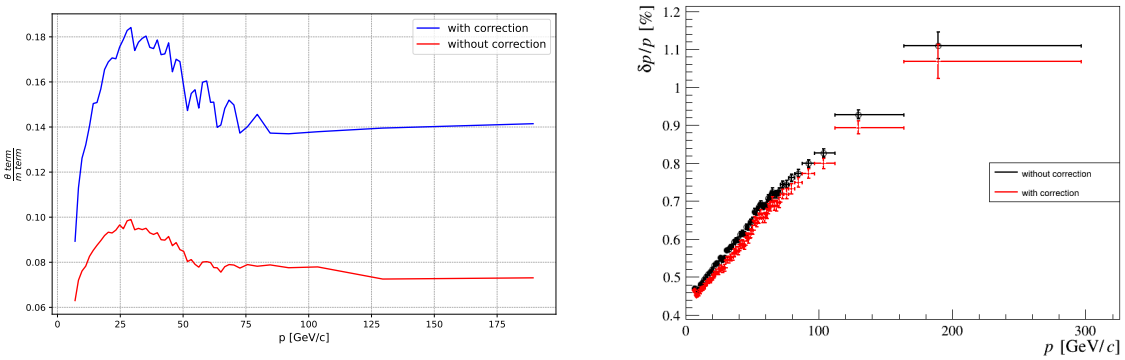

Figure 7: Left: the ratio between the θ term and the mass term becomes larger after the correction. Right: the momentum resolution becomes a bit smaller after the correction.

B Definition of variables used in HLT2 selection

Table 3: Definition of variables used in HLT2 selection.

Variable	Description
p_{T}	transverse momentum
PID_MU	log-likelihood difference between muon and pion hypotheses
MASS	invariant mass of particle
CHI2DOF	track χ^2 per degree of freedom
MINIPCHI2	minimum χ^2 of impact parameter
MINIP	minimum impact parameter
ISMUON	whether it's a muon
BPVDLS	decay length significance w.r.t. the best primary vertex
DOCACHI2	the χ^2 of the distance of the closest approach

References

[1] LHCb collaboration, R. Aaij *et al.*, *The LHCb Upgrade I*, JINST **19** (2024) P05065, arXiv:2305.10515.

[2] LHCb collaboration, A. A. Alves Jr. *et al.*, *The LHCb detector at the LHC*, JINST **3** (2008) S08005.

[3] LHCb collaboration, R. Aaij *et al.*, *LHCb detector performance*, Int. J. Mod. Phys. **A30** (2015) 1530022, arXiv:1412.6352.

[4] LHCb collaboration, *LHCb VELO Upgrade Technical Design Report*, CERN-LHCC-2013-021, 2013.

[5] LHCb collaboration, *LHCb Tracker Upgrade Technical Design Report*, CERN-LHCC-2014-001, 2014.

[6] M. Adinolfi *et al.*, *Performance of the LHCb RICH detector at the LHC*, Eur. Phys. J. **C73** (2013) 2431, arXiv:1211.6759.

[7] LHCb collaboration, *LHCb PID Upgrade Technical Design Report*, CERN-LHCC-2013-022, 2013.

[8] A. A. Alves Jr. *et al.*, *Performance of the LHCb muon system*, JINST **8** (2013) P02022, arXiv:1211.1346.

[9] LHCb collaboration, *LHCb Trigger and Online Upgrade Technical Design Report*, CERN-LHCC-2014-016, 2014.

[10] P. Li, E. Rodrigues, and S. Stahl, *Tracking Definitions and Conventions for Run 3 and Beyond*, LHCb-PUB-2021-005 (2021), CERN, Geneva.

[11] P. A. Günther, *Track Reconstruction Development and Commissioning for LHCb's Run 3 Real-time Analysis Trigger*, PhD thesis, Heidelberg University (2023).

[12] O. Callot and M. Schiller, *PatSeeding: A Standalone Track Reconstruction Algorithm*, LHCb-2008-042 (2008), CERN, Geneva.

[13] S. Aiola *et al.*, *HybridSeeding: A standalone track reconstruction algorithm for scintillating fibre tracker at LHCb*, Computer Physics Communications **260** (2021) 107713.

[14] R. M. Van der Eijk, *Track reconstruction in the LHCb experiment*, CERN-THESIS-2002-032, Amsterdam U. (2002).

[15] G. A. Cowan, D. C. Craik, and M. D. Needham, *Rapidsim: An application for the fast simulation of heavy-quark hadron decays*, Computer Physics Communications **214** (2017) 239–246.

[16] L. Anderlini *et al.*, *Muon identification for LHCb Run 3*, JINST **15** (2020) T12005, arXiv:2008.01579.

[17] LHCb collaboration, R. Aaij *et al.*, *Momentum scale calibration of the LHCb spectrometer*, JINST **19** (2024) P02008, arXiv:2312.01772.